Applied Physics Letters

Acoustic cloak designed by topology optimization for acoustic–elastic coupled systems

Cite as: Appl. Phys. Lett. **118**, 101102 (2021); https://doi.org/10.1063/5.0040911
Submitted: 17 December 2020 • Accepted: 18 February 2021 • Published Online: 08 March 2021

Garuda Fujii, Masayuki Takahashi and Youhei Akimoto

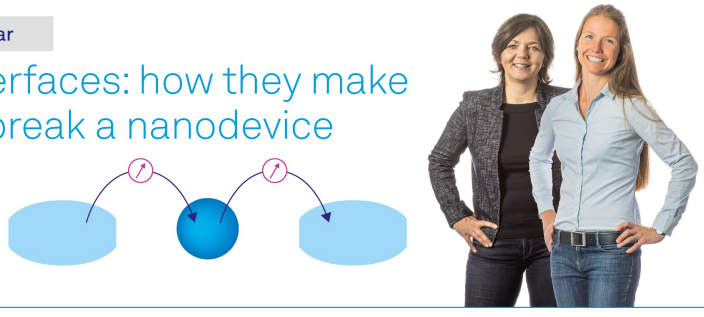

AIP Publishing

Applied Physics Letters ARTICLE scitation.org/journal/apl

Acoustic cloak designed by topology optimization for acoustic–elastic coupled systems

Cite as: Appl. Phys. Lett. **118**, 101102 (2021); doi: 10.1063/5.0040911
Submitted: 17 December 2020 · Accepted: 18 February 2021 ·
Published Online: 8 March 2021

Garuda Fujii,[1,a)] Masayuki Takahashi,[2] and Youhei Akimoto[3]

AFFILIATIONS

[1]Institute of Engineering, Shinshu University, Nagano 380-8553, Japan
[2]Seiko Epson Corporation, 3-3-5 Owa, Suwa, Nagano 392-8502, Japan
[3]Faculty of Engineering, Information and Systems, University of Tsukuba and RIKEN AIP, 1-1-1 Tennodai, Tsukuba 305-8573, Japan

Note: This Paper is part of the APL Special Collection on Metastructures: From Physics to Applications.
[a)]**Author to whom correspondence should be addressed:** g_fujii@shinshu-u.ac.jp

ABSTRACT

By including acoustic-elastic interactions in a topology optimization based on the covariance matrix adaptation evolution strategy, we developed acoustic cloaks of optimal design that render an object unobservable through airborne and water-borne sounds. This strategy helps in exploring optimal topologies that minimize the scattering of airborne and water-borne sounds around acoustic cloaks made from acrylonitrile butadiene styrene copolymers frequently used as *ink* in 3D printers. By applying level set methods, our designed cloaks are expressed as iso-surfaces representing the sharp structural boundaries between the acoustic and elastic media. On these boundaries, conditions that couple the elastic and acoustic aspects of the scattering are imposed. Furthermore, our cloak designs ensure that scatterers are unobservable to sound waves of multiple frequencies incident from various angles by minimizing the fitness incorporating multiple objective functions under several structural symmetries.

Since the pioneering work on acoustic cloaking,[1] transformation acoustics and acoustic metamaterials[2,3] cover the main approaches to achieve the acoustic cloaking. Nonetheless, scattering cancelation[4,5] has attracted some attention as a practical approach for achieving acoustic cloaks. Structural optimization is a very effective method to determine the underlying structures of schemes to achieve a specific performance and has been applied to the overall design of acoustic cloaks, enabling scattering cancelations that improve cloaking performance. An acoustic cloak composed of cylinders has been designed,[6] and the approach was extended to toroidal structures in 3D.[7] Shape optimization for an acoustic cloak was presented based on Bézier curves[8] and boundary element analysis.[9]

Topology optimization[10] is the most flexible means to optimize structures for improving their performance in that not only changes in shape but also *topological changes* including creating holes that are allowed. For acoustic cloaking, topology optimization has yielded structural designs based on the density method with a material mask overlay scheme.[11] However, the optimization proceeds by optimizing the positions and radii of cylinders for cloaking without changing the structural topology. Later, level set-based topology optimization for acoustic cloaks[12] and a density-based one for acoustic cloaks in the presence of background mean flows[13] were proposed. Recently, topological structural designs of acoustic cloaks amid the uncertainty in material properties or manufacturing were developed.[14] However, despite the fact that, in general, scattering cancelation allows sound to penetrate acoustic cloaks and the scatterer itself, the above topology optimizations for acoustic cloaks ignored the intrusion of sound into the elastic body by assuming that its surfaces completely reflected acoustic waves. Only stiff and dense materials, such as metals in air, satisfy this assumption, i.e., modeling elastic bodies as rigid bodies. *Underwater* acoustic cloaking cannot be designed in this manner. Even in cloaking for airborne sound, only a narrow selection of materials is available with which to construct such cloaks.

To overcome this problem, we present a topology optimization incorporating acoustic-elastic interactions in the computational design of acoustic cloaks. Topology-optimized metastructures made of acrylonitrile butadiene styrene (ABS) are developed, which cancel ambient acoustic scattering waves in both air and water. By incorporating an acoustic-elastic interaction together with the acoustic and elastic properties of materials in topology optimization,[15,16] the acoustic wave equation and the dynamic equilibrium equation were numerically solved for the acoustic and elastic media, respectively. Therefore,

designers can arbitrarily choose an ambient acoustic medium and elastic materials in structuring acoustic cloaks. Moreover, by incorporating such interactions, simulating the effect of holes in the elastic body on the surrounding acoustic field becomes possible. Hence, benefits accrue from topological changes, i.e., hole creation, which improve the physical performance of such cloaks.

For acoustic-elastic coupled cloaking problems [Fig. 1(a)], topology optimization involves minimizing the acoustic scattering produced by an obstacle Ω_{obs}, here made of aluminum; the fixed design domain Ω_D, in which the ABS structure Ω_e is transformed to affect acoustic cloaking, is set to cover Ω_{obs}. We simulate the acoustic scattering in an open region; the perfectly matched layer, Ω_{PML}, is configured to implement the absorbing boundary condition. The entire analysis domain is rectangular, with the length in the y direction being smaller, specifically, $L_y = L_x \times 2/3$ to reduce the area under analysis and, hence, the computational cost. Boundary conditions imposed at the acoustic-elastic interfaces account for the acoustic-elastic interactions and effectively couple the governing equations describing the elastic vibrations and acoustic waves. The interfaces between the acoustic medium and the elastic media are expressed as iso-surfaces of a level set function [Fig. 1(b)], along which finite elements are created for the numerical modeling.

The elastic material of the cloak occupies Ω_e and minimizes the acoustic scattering in the outer domain Ω_{out}. The objective function determining the design of the acoustic cloak is defined as

$$\Psi_X = \frac{1}{\Psi_X^n}\int_{\Omega_{out}} |p^s|^2 d\Omega, \tag{1}$$

where p^s represents the sound pressure of the scattered wave and the total acoustic pressure is given as $p = p^s + p^i$, with p^i denoting the sound pressure of the incident wave. Subscript $X = (a, w)$ indicates the acoustic medium for airborne and water-borne sounds. Ψ_X denotes the corresponding objective function, with its normalization Ψ_X^n being

$$\Psi_X^n = \int_{\Omega_{out}} |p^s_{bare}|^2 d\Omega, \tag{2}$$

where p^s_{bare} denotes the scattered sound pressure from the bare cylinder with no cloak present. The governing equations for sound pressure p in the acoustic medium and the stress σ_{ij} and displacements u_i in the elastic media are

$$\rho_a^{-1} p_{,ii} + \omega^2 \kappa_a^{-1} p = 0 \quad \text{in } \Omega_D \backslash \Omega_e, \Omega_{out}, \tag{3}$$

$$\sigma_{ji,j} + \rho_e \omega^2 u_i = 0 \quad \text{in } \Omega_e, \Omega_{obs}, \tag{4}$$

where ρ_a and ρ_e are the densities of the acoustic and elastic media, ω is the angular frequency of the acoustic wave, and κ_a is the bulk modulus of an acoustic medium; here, Einstein's summation convention is used. At the interface between the two media, the boundary conditions are

$$p_{,i} n_i^a = -\omega^2 \rho_a u_i n_i^e \quad \text{on } \Gamma_e^a, \Gamma_{obs}^a, \tag{5}$$

$$\sigma_{ji}(\boldsymbol{u}) n_i^e = p n_i^a \quad \text{on } \Gamma_e^a, \Gamma_{obs}^a, \tag{6}$$

where n_i^a and n_i^e represent the outward unit vectors normal to the boundaries of the acoustic and elastic domains [Fig. 1(b)], respectively, with the vectors satisfying $n_i^a = -n_i^e$, and $\boldsymbol{u}$ is the displacement vector. The above boundary conditions are assigned to the integral terms along the boundaries in the weak form derived from the governing equations in Eqs. (3) and (4) in the finite-element analysis. For simplicity, we assume the elastic domain and that of the cloaked obstacle, Ω_e and Ω_{obs}, to be joined, and continuity of the displacement and that of the normal component of stress apply at the interface Γ_{obs}^e. The above governing equations and the boundary conditions for acoustic and elastic wave are different from those for electromagnetic waves[17] and heat transfer.[18] Numerical analysis for acoustic-elastic coupled systems becomes a multiphysics problem in which the governing equations pertaining to the acoustic and elastic domains differ. The problem results in a system of algebraic equations with an asymmetric matrix that is solved in finite-element analysis. Table I lists the material parameters used in our topology optimization.

The acoustic and elastic domains, $\Omega_D \backslash \Omega_e$ and Ω_e, are represented by a level set function $\phi(\boldsymbol{x})$, which is a continuous scalar variable defined over Ω_D expressing the structure explicitly. In the present

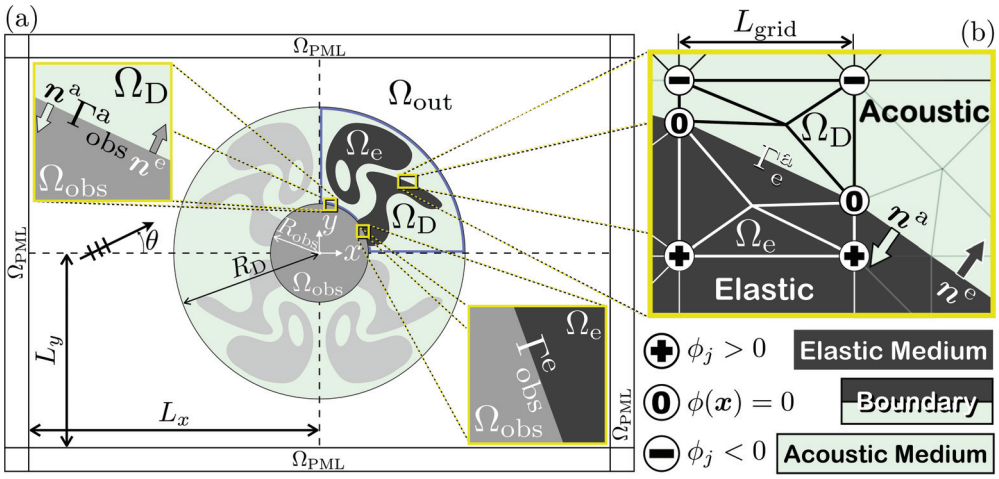

FIG. 1. (a) Schematic of an acoustic-elastic coupled topology optimization problem for an acoustic cloak. Each domain size is set to $R_{obs} = R_D/3$, $L_x = R_D \times 2$, $L_y = R_D \times 4/3$, and $L_{grid} = R_D/75$. (b) Discretized level set functions and the interfaces between the acoustic medium and the elastic media.

TABLE I. Elastic and acoustic properties in the optimization.

Elastic property	ABS (Ω_e)	Aluminum (Ω_{obs})
Density	1.02 Mg/m^3	2.70 Mg/m^3
Young's modulus	2.40 GPa	69.0 GPa
Poisson's ratio	0.393	0.334
Acoustic property	Air ($\Omega_D\backslash\Omega_e$, Ω_{out})	Water ($\Omega_D\backslash\Omega_e$, Ω_{out})
Density	1.20 kg/m^3	1.00 Mg/m^3
Bulk modulus	142 kPa	2.25 GPa

problem, the function becomes positive in the elastic domain Ω_e, negative in the acoustic domain $\Omega_D\backslash\Omega_e$, and zero at the interface between the elastic and acoustic domains Γ_e^a [see Fig. 1(b)] and defined as

$$\begin{aligned}\Omega_D\backslash\Omega_e &= \{\boldsymbol{x}\,|\,-1 \le \phi(\boldsymbol{x}) < 0\},\\ \Gamma_e^a &= \{\boldsymbol{x}\,|\,\phi(\boldsymbol{x}) = 0\},\\ \Omega_e\backslash\Gamma_e^a &= \{\boldsymbol{x}\,|\,0 < \phi(\boldsymbol{x}) \le 1\}.\end{aligned} \tag{7}$$

Here, the interface between the acoustic and elastic media Γ_e^a is expressible as an iso-surface of the level set function. The optimal $\boldsymbol{\phi} = \{\phi_1, \ldots, \phi_j, \ldots, \phi_n\}$, the set of discretized level set functions, is explored by covariance matrix adaptation evolution strategy (CMA-ES)[19] with the box-constraint handling,[17] $-1 \le \phi_j \le 1$, for infimizing the regularized fitness,

$$\inf_{\phi} \quad F_r = \max(\Psi_X, \tau L_p), \tag{8}$$

where L_p denotes the normalized perimeter of the structure and τ the regularization coefficient determining the ratio between Ψ_X and L_p.

Figures 2(a)–2(c) and 2(d)–2(f) illustrate acoustic scattering by a bare aluminum cylinder in air and water, respectively. The acoustic wave in air is scattered intensively at the cylinder's surface, and stress is induced in the cylinder by the sound pressure [Fig. 2(b)]. With only the cylinder present, water-borne sound is also scattered, but its interference pattern [Fig. 2(e)] is different from that for airborne sound [Fig. 2(b)]. The difference stems from differences in material properties of air and water (Table I).

Despite the scatterer, both topology-optimized acoustic cloaks [Figs. 3(a) and 3(d)] can reproduce the acoustic plane wave flowing around it with little scattering in Ω_{out} [Figs. 3(b) and 3(e)]. The thinness of the cloaking shell, $R_D - R_{obs} = \frac{2}{3}R_D$, is about 1.67 times the operating wavelength in acoustic medium λ because $R_D = 2.5\lambda$ derived from $\frac{\omega R_D}{2\pi c_a} = \frac{R_D}{\lambda} = 2.5$. Topology optimization under the *stronger* perimeter constraint, $\tau = 1 \times 10^{-2}$ [Figs. 3(a)–3(c)], provides a simple optimal configuration with a smaller perimeter, $L_p = 39.6$ [Fig. 3(a)], than the optimal configuration with $L_p = 80.7$ [Fig. 3(d)] obtained under the *weaker* perimeter constraint, $\tau = 1 \times 10^{-3}$ [Figs. 3(d)–3(f)]. This constraint permits more complex optimal configurations and prioritizes enhancements in the performance of the acoustic cloaking during optimization. Indeed, the value of the objective function [Figs. 3(d)–3(f)] reaches $\Psi_a = 7.00 \times 10^{-2}$, that is, the scattering intensity in Ω_{out} was reduced to 7.00% of that when just the scatterer is present in air without the cloak [Figs. 2(a)–2(c)]. To increase the sound propagation angle at which the cloak works,

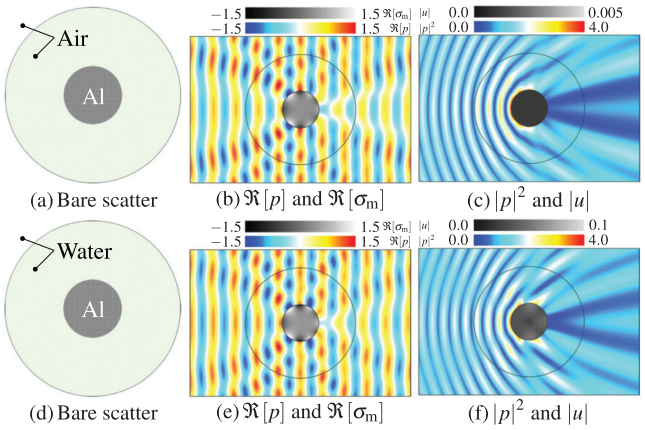

FIG. 2. (a) and (d) A bare aluminum cylinder, (b) and (e) sound pressure of the total acoustic wave, $\Re[p] = \Re[p^s_{bare} + p^i]$ in $\Omega_D\backslash\Omega_e$ and Ω_{out}, and mean stress, $\Re[\sigma_m] = \Re[\sigma_{ii}]/2$ in Ω_e and Ω_{obs}, (c) and (f) squared pressure norm of the total wave, $|p|^2$ in $\Omega_D\backslash\Omega_e$ and Ω_{out}, and magnitude of the displacement, $|u|$ in Ω_e and Ω_{obs}, in (a)–(c) air and (d)–(f) water. The value of the objective function is (a)–(c) $\Psi_a = 1.00 \times 10^0$ and (d)–(f) $\Psi_w = 1.00 \times 10^0$. The incident acoustic plane wave oscillates at normalized frequency (b) and (c) $\omega R_D/2\pi c_a = 2.5$ and (e) and (f) $\omega R_D/2\pi c_w = 2.5$ (c_a and c_w denote the speed of sound in air and water, respectively).

topology optimizations under structural symmetries imposed about not only the x and y axes but also the diagonals $y = \pm x$ were performed [Fig. 4]. From the optimum configurations obtained subject to the structural symmetries present [Figs. 4(a) and 4(d)], an improved performance is exhibited in Fig. 4 compared with that in Fig. 3 despite the increase in structural symmetry. These additional symmetries not only contribute to the increase in the sound propagation angle at which the cloak works but also reduce the number of design variables from $n = 3982$ to $n = 2009$, thereby accelerating the exploration of optimal topologies minimizing F_r through the CMA-ES.

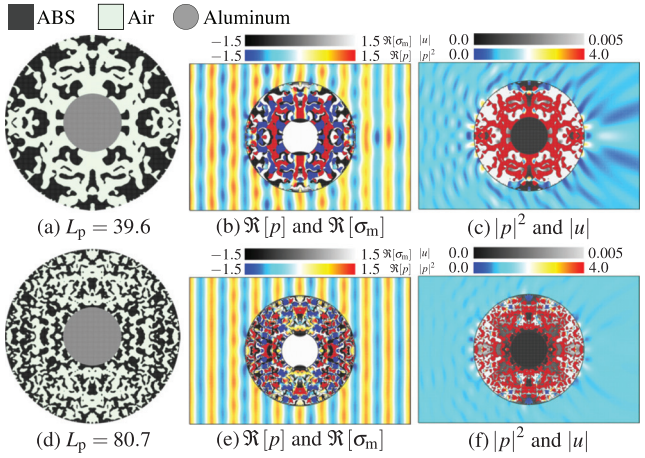

FIG. 3. Topology-optimized acoustic cloaks for *airborne* sound obtained when (a)–(c) $\tau = 1 \times 10^{-2}$ and (d)–(f) $\tau = 1 \times 10^{-3}$ and their cloaking performance. The value of the objective function is (a)–(c) $\Psi_a = 3.45 \times 10^{-1}$ and (d)–(f) $\Psi_a = 7.00 \times 10^{-2}$.

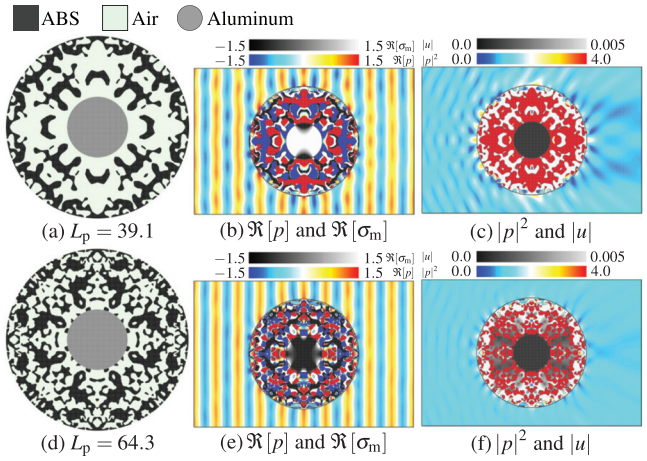

FIG. 4. Multidirectional acoustic cloaks for airborne sound under structural symmetries imposed about the x, y, and $y = \pm x$ axes and their cloaking performance. The regularization coefficient is set to (a)–(c) $\tau = 1 \times 10^{-2}$ and (d)–(f) $\tau = 1 \times 10^{-3}$. The value of the objective function is (a)–(c) $\Psi_a = 3.26 \times 10^{-1}$ and (d)–(f) $\Psi_a = 6.26 \times 10^{-2}$.

Underwater applications clearly need to incorporate an acoustic-elastic interaction when numerically simulating acoustic scattering in water.[20] For this reason, we next demonstrate topology optimization for such situations (Fig. 5) and those subject to additional structural symmetry about the diagonals $y = \pm x$ (Fig. 6). The squared pressure norm of *airborne* sound [Figs. 3(c) and 3(f) and 4(c) and 4(f)] becomes strong (red) almost everywhere in the air within the ABS, whereas the squared norm of the pressure of *water-borne* sound in water within the ABS vanishes or is close to zero (blue) at most of the Ω_D [Figs. 5(c) and 5(f) and 6(c) and 6(f)]. With the reduction of design variable values, more promising optimal configurations were obtained in terms of both performance and structural simplicity with smaller L_p, cf. results in Figs. 5 and 6.

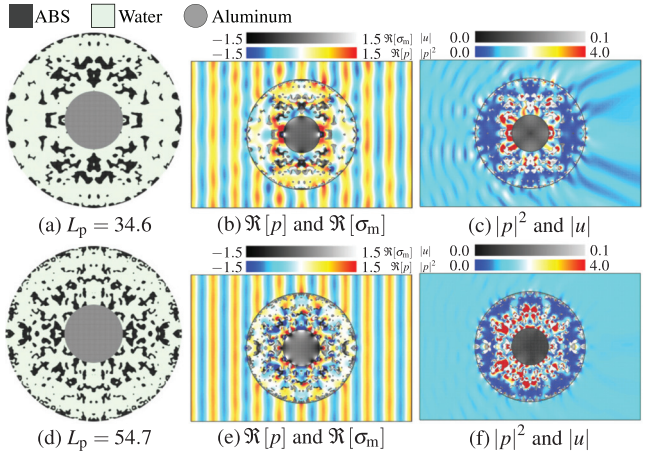

FIG. 5. Topology-optimized *underwater* acoustic cloaks designed setting (a)–(c) $\tau = 1 \times 10^{-2}$ and (d)–(f) $\tau = 1 \times 10^{-3}$ and their cloaking performance. The value of the objective function is (a)–(c) $\Psi_w = 3.42 \times 10^{-1}$ and (d)–(f) $\Psi_w = 5.12 \times 10^{-2}$.

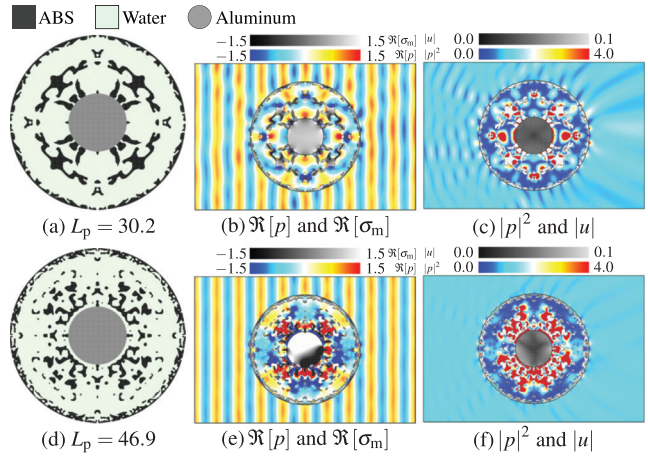

FIG. 6. Multidirectional underwater cloaks obtained from topology optimization with structural symmetries imposed about the x, y, and $y = \pm x$ axes and sound pressure distributions of water-borne sound around the cloaks. The regularization coefficient is set to (a)–(c) $\tau = 1 \times 10^{-2}$ and (d)–(f) $\tau = 1 \times 10^{-3}$. The value of the objective function is (a)–(c) $\Psi_w = 2.81 \times 10^{-1}$ and (d)–(f) $\Psi_w = 4.45 \times 10^{-2}$.

From changes in the objective function with respect to the incidence angle and sound frequency (Fig. 7), increases in the propagation angle at which the cloak works for airborne and water-borne sounds were obtained as intended when diagonal structural symmetries were imposed [Figs. 7(a) and 7(b)] although acoustic invisibility for airborne sound was only possible within a very narrow range of frequencies [Fig. 7(c)]. For underwater cloaking [Fig. 7(d)], the frequency range of acoustic invisibility is slightly wider than that for acoustic cloaking of airborne sound [Fig. 7(c)]. However, the optimized performance is not robust to fluctuations in frequency of sound waves.

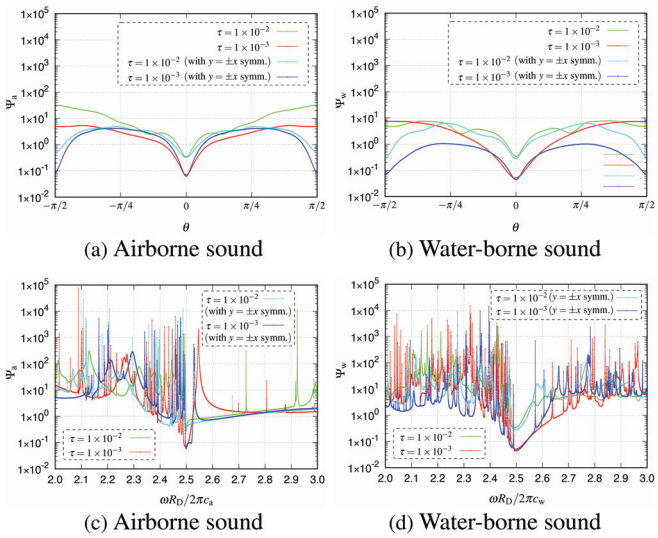

FIG. 7. (a) and (b) Incident angle and (c) and (d) frequency responses with regard to the performance of acoustic cloaks designed for (a) and (c) airborne and (b) and (d) water-borne sounds.

The frequencies of the diverging peaks correspond to the eigenfrequencies of the acoustic-elastic coupled system for cloaking. Reducing these peaks from a specific range of frequencies may be possible by applying an eigenvalue analysis and conditional value at risk.[21] In practice, removing all peaks of the objective function is very difficult because of the computational cost and physical difficulty. Nevertheless, to achieve cloaking at multiple specific frequencies is worth trying.

For a wider frequency range of acoustic invisibility, we performed topology optimizations to reduce the acoustic scattering at multiple frequencies and infimize redefined fitness,

$$\inf_{\phi} \quad F_{\max} = \max(\Psi_X^{\omega_1^n}, \Psi_X^{\omega_2^n}, \Psi_X^{\omega_3^n}) + \tau L_p, \tag{9}$$

where $\Psi_X^{\omega_i^n}$ denotes the objective function for acoustic waves in medium X oscillating at the normalized frequency $\omega_i^n = \omega_i R_D/2\pi c_X$, with i indexing its frequencies and c_X its speed of sound.

Multidirectional acoustic cloaks for *airborne* sound oscillating at multiple frequencies are obtained by minimizing $F_{\max}$ [Fig. 8(a)]. For *underwater* cloaking, topology-optimized designs involving $F_{\max}$ can suppress acoustic scattering waves at three sets of frequencies; see Figs. 8(b)–8(d). In optimized structures for cloaking airborne and water-borne sound, a fine structure remains as a common structural feature. Because this fine structure is necessary to realize wider frequency bands, its retention is thought to arise despite the perimeter constraint during the optimization computation. By imposing the minimum length scale,[22] the fine structures in optimal configurations may possibly be removed, but performances may worsen. From the cloaking performance of optimal configurations for airborne and water-borne sounds over a wide range of frequencies [Figs. 8(e) and 8(f), respectively], the frequency range has clearly been extended by minimizing $F_{\max}$. The optimal configurations for underwater cloaking [Figs. 8(b) and 8(c)] also exhibit a "frequency band" for low values of the objective function [Fig. 8(f)]. Only the optimal configurations obtained for the widest ranges of frequency [Fig. 8(d)] do not have an "unobservable frequency band" but exhibit low values of the objective function at three specific frequencies, i.e., $\omega R_D/2\pi c_w = 2.0$, 2.5, and 3.0.

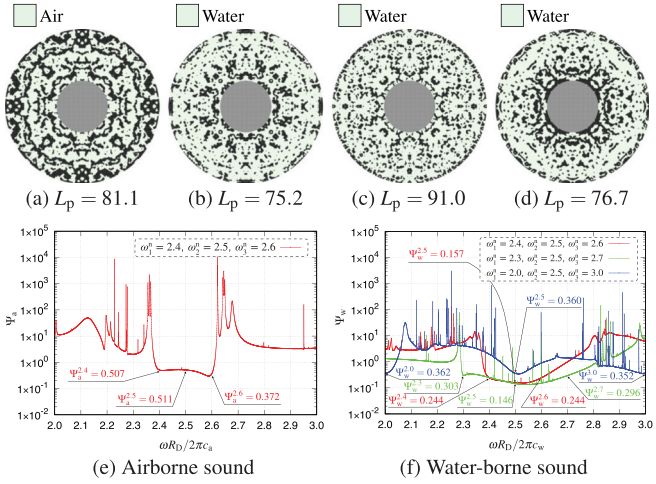

FIG. 8. Multidirectional acoustic cloak for manipulating (a) airborne and (b)–(d) water-borne sounds oscillating at multiple frequencies obtained by minimizing $F_{\max}$ with $\tau = 1 \times 10^{-2}$ and symmetries about the x, y, and $y = \pm x$. Frequencies are set to (a) $\omega R_D/2\pi c_a = 2.4$, 2.5, and 2.6, (b) $\omega R_D/2\pi c_w = 2.4$, 2.5, and 2.6, (c) $\omega R_D/2\pi c_w = 2.3$, 2.5, and 2.7, and (d) $\omega R_D/2\pi c_w = 2.0$, 2.5, and 3.0. Frequency response associated with performance of the optimum configurations for (e) airborne sound and (f) water-borne sound.

By applying topology optimization for acoustic-elastic coupled systems to the design of acoustic cloaks, we can employ arbitrary materials in constructing the acoustic cloaks. However, the question then is how do the elastic properties of these materials affect the cloaking performance for *airborne* sound? We investigated the effect of materials on cloaking performance (see the supplementary material). When sound is scattered only once in a system with a bare scatter, there is little difference between airborne sound scattered by bare cylinders made of aluminum, ABS, and a rigid material (Fig. S1). However, when an optimized cloak surrounds the cylinder, performance is affected by the elastic properties of materials composing the acoustic cloak (Fig. S2). In these systems, multiple scattering occurs among the elastic structures and the sound pressure is enhanced through wave interference. The stress in the elastic materials is also increased by the enhanced ambient sound pressure around the elastic body (Figs. 3, 4, and S2), and thereby, the elastic properties of the material affect cloaking performance. In the experiment,[8] we found good agreement with the rigid body approximation for the ABS. However, changing the material from the ABS assumed in the optimization to aluminum or a rigid body produces a performance deterioration even if the change is within allowable tolerances. Therefore, inclusion of an acoustic-elastic interaction in the design of the acoustic cloak for airborne sound is worthwhile. The rigid body approximation model of an elastic body may be refined by reducing the sound pressure among the elastic bodies, specifically, adding to the fitness a term containing the square norm of sound pressure placing a stress on the elastic structure, namely, $\int_{\Omega_D \setminus \Omega_e} |p|^2 d\Omega$, to F_r.

In this study of acoustic-elastic coupled cloaking, the structural topology of acoustic cloaks was optimized using CMA-ES-based topology optimization using the sharp interface modeling by the level set method. Optimal configurations for cloaking airborne and water-borne sound were presented. Boundary conditions imposed on the interface to take into account acoustic-elastic interactions led to a coupling of the elastic and acoustic problems. By infimizing the acoustic scattering at multiple frequencies under different structural symmetries, cloaks designed to operate for airborne or water-borne sounds are possible over a wider range of frequencies and incidence angles. The optimal acoustic cloaks presented are expected to be demonstrated experimentally as well as the electromagnetic cloak,[23] and our computational design scheme may be applied to promising metadevices such as the biphysical cloak[24] and in the area of undetectable sensing.[25,26]

See the supplementary material for the effect of materials on cloaking performance.

We thank Richard Haase, Ph.D., from Edanz Group (https://en-author-services.edanz.com/ac) for editing a draft of this manuscript.

DATA AVAILABILITY

The data that support the findings of this study are available from the corresponding author upon reasonable request.

REFERENCES

[1]S. A. Cummer and D. Schurig, New J. Phys. **9**, 45 (2007).
[2]S. A. Cummer, J. Christensen, and A. Alù, Nat. Rev. Mater. **1**, 16001 (2016).
[3]M. R. Haberman and M. Guild, Phys. Today **69**(6), 42 (2016).
[4]M. D. Guild, M. R. Haberman, and A. Alù, J. Acoust. Soc. Am. **128**, 2374 (2010).
[5]M. D. Guild, A. Alù, and M. R. Haberman, J. Acoust. Soc. Am. **129**, 1355 (2011).
[6]V. M. García-Chocano, L. Sanchis, A. Díaz-Rubio, J. Martínez-Pastor, F. Cervera, R. Llopis-Pontiveros, and J. Sánchez-Dehesa, Appl. Phys. Lett. **99**, 074102 (2011).
[7]L. Sanchis, V. M. García-Chocano, R. Llopis-Pontiveros, A. Climente, J. Martínez-Pastor, F. Cervera, and J. Sánchez-Dehesa, Phys. Rev. Lett. **110**, 124301 (2013).
[8]Z. Lu, L. Sanchis, J. Wen, L. Cai, Y. Bi, and J. Sánchez-Dehesa, Sci. Rep. **8**, 12924 (2018).
[9]P. R. Andersen, V. C. Henriquez, L. Sanchis, and J. Sánchez-Dehesa, in Proceedings of the International Congresses on Acoustics (2019), pp. 5600–5606.
[10]M. P. Bendsøe and N. Kikuchi, Comput. Methods Appl. Mech. Eng. **71**, 197 (1988).
[11]J. Andkjær and O. Sigmund, J. Vib. Acoust. **135**, 041011 (2013).
[12]M. Takahashi, Y. Akimoto, and G. Fujii, Trans. Jpn. Soc. Mech. Eng. **84**(859), 17-00590 (2018).
[13]Z. Ma, O. Stalnov, and X. Huang, Acta Mech. Sin. **35**, 964 (2019).
[14]P. Chen, M. R. Haberman, and O. Ghattas, J. Comput. Phys. **431**, 110114 (2021).
[15]C. B. Dilgen, S. B. Dilgen, N. Aage, and J. S. Jensen, Struct. Multidisc. Optim. **60**, 779 (2019).
[16]Y. Noguchi, T. Yamada, K. Izui, and S. Nishiwaki, "Optimum design of an acoustic metamaterial with negative bulk modulus in an acoustic-elastic coupled system using a level set-based topology optimization method,„" Int. J. Numer. Meth. Eng. **113**(8), 1300–1339 (2018).
[17]G. Fujii, M. Takahashi, and Y. Akimoto, Comput. Methods Appl. Mech. Eng. **332**, 624 (2018).
[18]G. Fujii, Y. Akimoto, and M. Takahashi, Appl. Phys. Lett. **112**, 061108 (2018).
[19]N. Hansen and A. Ostermeier, Evol. Comput. **9**, 159 (2001).
[20]Y. Chen, M. Zheng, X. Liu, Y. Bi, Z. Sun, P. Xiang, J. Yang, and G. Hu, Phys. Rev. B **95**, 180104 (2017).
[21]R. T. Rockafellar and S. Uryasev, J. Risk **2**, 21 (2000).
[22]J. K. Guest, J. H. Prévost, and T. Belytschko, Int. J. Numer. Methods Eng. **61**, 238 (2004).
[23]L. Lan, F. Sun, Y. Liu, C. K. Ong, and Y. Ma, Appl. Phys. Lett. **103**, 121113 (2013).
[24]Y. Zhou, J. Chen, L. Liu, Z. Fan, and Y. Ma, NPG Asia Mater. **12**, 27 (2020).
[25]A. Alù and N. Engheta, Phys. Rev. Lett. **102**, 233901 (2009).
[26]M. D. Guild, A. Alù, and M. R. Haberman, Appl. Phys. Lett. **105**, 023510 (2014).